We are IntechOpen,
the world's leading publisher of
Open Access books
Built by scientists, for scientists

4,800
Open access books available

122,000
International authors and editors

135M
Downloads

Our authors are among the

154
Countries delivered to

TOP 1%
most cited scientists

12.2%
Contributors from top 500 universities

CLARIVATE ANALYTICS
BOOK CITATION INDEX
INDEXED

WEB OF SCIENCE™

Selection of our books indexed in the Book Citation Index
in Web of Science™ Core Collection (BKCI)

Interested in publishing with us?
Contact book.department@intechopen.com

Numbers displayed above are based on latest data collected.
For more information visit www.intechopen.com

Coastal Disasters and Remote Sensing Monitoring Methods

Yan Yu, Shengbo Chen, Tianqi Lu and Siyu Tian

Abstract

Coastal disaster is abnormal changes caused by climate change, human activities, geological movement or natural environment changes. According to formation cause, marine disasters as storm surges, waves, Tsunami coastal erosion, sea-level rise, red tide, seawater intrusion, marine oil spill and soil salinization. Remote sensing technology has real-time and large-area advantages in promoting the monitoring and forecast ability of coastal disaster. Relative to natural disasters, ones caused by human factors are more likely to be monitored and prevented. In this paper, we use several remote sensing methods to monitor or forecast three kinds of coastal disaster cause by human factors including red tide, sea-level rise and oil spilling, and make proposals for infrastructure based on the research results. The chosen method of monitoring red tide by inversing chlorophyll-a concentration is improved OC3M Model, which is more suitable for the coastal zone and higher spatial resolution than the MODIS chlorophyll-a production. We monitor the sea-level rise in coastal zone through coastline changes without artificial modifications. The improved Lagrangian model can simulate the trajectory of oil slick efficiently. Making the infrastructure planning according the coastal disasters and features of coastline contributes to prevent coastal disaster and coastal ecosystem protection. Multi-source remote sensing data can effectively monitor and prevent coastal disaster, and provide planning advices for coastal infrastructure construction.

Keywords: chlorophyll-a, coastline, oil spilling, monitoring, forecast, coastal infrastructure, multi-source

1. Introduction

The coastal zone is the intersection zone of the lithosphere, hydrosphere, biosphere and atmosphere interaction where the continent connects with the ocean. The disaster in the coastal

zone is abnormal changes caused by climate change, human activities, geological movement or natural environment changes. According to morphology, marine disasters could be classified as disastrous waves, sea ice, red tide, Tsunami and storm tide. According to formation cause, marine disasters as storm surges, waves, Tsunami coastal erosion, sea-level rise, red tide, seawater intrusion, marine oil spill and soil salinization. Most common marine disasters happened in coastal areas of China are coastal disaster, storm tide, seawater intrusion, disastrous wave, Tsunami and so on. These disasters caused great loss to the residents of coastal areas, economic and ecological environment. Besides, the disaster caused by human activities has become more and more serious, such as red tide, rising sea-level and ocean oil spill. With the development of satellite technology, remote sensing technology has gradually become an important means for monitoring coastal disasters and environmental changes that and providing data source for coastal infrastructure planning. Climate and ecological change caused by human activities is a hot issue of social concern at present. Taken Bohai Bay located in the South China Sea as an example, this paper will discuss remote sensing method to monitor and prevent three coastal disasters including red tide and, sea-level rise and oil spill, which could be applied in coastal infrastructure planning.

Satellite remote sensing technology can monitor and prevent inshore disasters in large area scale and in real time, which has been successfully applied in monitoring red tide, sea-level rise and marine oil spill. Taking effective measures to prevent the occurrence or control the area of red tide before its outburst is a long-term goal of red tide management. In 1950s, the red tide often strikes the coastal areas of industrially developed countries such as the USA and Western Europe, and the research on red tide has been conducted earlier, which mainly focuses on statistics in the red tide causes, ecotoxicology, monitoring management and so on. Doucette et al. [1] carried out toxicological studies on the nutrient conditions under the red tide. Moisn [2] investigates the effect of temperature on the growth rate of red tide organisms. Temperature and nutrient salts are the main factors in the formation of red tide. Based on the water temperature of red tide, Huang and Lou [3] is established the artificial neural network method, but the rise of flow region with low temperature could also result in the red tide, so extracting red tide through water temperature has rather great limitation. Based on the water temperature of red tide, Huang and Lou [3] established the artificial neural network method, but the rise of flow region with low temperature could also result in the red tide, so extracting red tide through water temperature has rather great limitation. Autotrophic algae photosynthesis is the main energy source of most red tide, and the cell have abundant chlorophyll, thus the red tide could be identified through abnormal increase of chlorophyll content. Steidinger & Haddad [4] used CZCS (Coastal Zone Color Scanner) algorithm to obtain chlorophyll content to identify the short bloom dinoflagellate blooms in the western waters of the Florida shelf in 1981. The CZCS algorithm has been successfully applied in Case1 water. There exist 10 algorithms calculated from the ratio of blue and green using water color sensors like MODIS, SeaWiFS, MERIS, OCTS [5]. However, the effect of traditional algorithms of Case 2 is not so good because of suspended sediment. Based on the relative reflectance spectra of red tide algae measured in the East China Sea, Mao and Huang [6] proposed a combination method of three bands for eliminating the disturbance of suspended sediment on the retrieval of chlorophyll concentration. Chlorophyll empirical

algorithm is too simple to consider the absorption and scattering properties of water and bio optical model. The semi empirical considers the absorption and scattering coefficient of different group of water (chlorophyll, seawater, suspended sediment, CDOM) of [7–9] in Case 2 algorithm using CZCS. The inversion of coastal chlorophyll is limited by the spatial resolution, for example MODIS with spatial resolution of data could not meet the inversion requirements though the spectral resolution is high, so this paper adopts experimental algorithm that uses band 1 and band 2 of MODIS with resolution of 500 m, proposed by Fan et al., using, this algorithm is more consistent with the requirements of offshore chlorophyll inversion, which is more suitable for chlorophyll inversion.

Inter Government Panel on Climate Change (IPCC) has been assessing the impact of global climate change on natural ecology and human socio-economic systems five times since 1990 [10]. IPCC's fourth report on climate change (AR4) pointed out that since 1961, the global average sea-level rise as the rate of 1.8 mm/a, and by 1993, this data has increased by 3.1 mm/a. Over the past 30 years, China's average annual sea-level rise as the rate of 2.9 mm/a. Melting glaciers is the main reason of rising sea-level since 1960s. Asian glaciers that has the core of Qinghai Tibet plateau continue to retreat [11, 12]; in the past 20 years, the Antarctic ice sheet and the Greenland ice sheet keep melting, and the ablation rate continues to accelerate, leading to rising sea-level [13–15]. Sea-level rise caused by global climate change have significant impact on the coast. The coastal area exerts most important influence on social and economic development, is also the most serious and direct area affected by sea-level changes. More than about half of the world population, production and consumption are distributed in the coastal areas within the shoreline, and most of the world's wealth are concentrated in the regional economy. Monitoring the coastline changes for many years by remote sensing images can help to analyze the impact of sea-level rise on different types of coastline. The coastline extraction can be divided into automatic extraction and visual interpretation. Bouchahma et al. [16] applied Canny operator to binary NDWI from Landsat TM. Xu [17] proposed the modified normalized difference water index MNDWI (Modified NDWI), the NDWI index in the near infrared band is replaced by infrared band to get better accurate extraction for water information. But most methods are not perfect in the extraction of biological shoreline and mud shoreline. In the coastal areas with smaller scales, high resolution remote sensing data can be used for visual interpretation for different types of coastline, and better results can be obtained. With the rapid development of Marine transportation and offshore oil development, the high frequency of the oil spill accidents has caused a lot of damage to the coastal ecological environment. There are several commonly used operational oil spill models, such as MOTHY (Modèle Océanique de Transport d'Hydrocarbures, a French operational oil spill drift forecast system), OSCAR (Oil Spill Contingency and Response), OILMAP (Oil Spill Model 30 and Response System), ADIOS2 (Automated Data Inquiry for Oil Spills), GNOME (General NOAA Operational Modeling Environment) [18, 19]. The models above have several parameters, such as wind, current and waves are affected by different environment. Thus, it is necessary to calibrate Lagrangian transport model to get the optimal model coefficients for certain oil spill accident with the special datasets. Tian et al. [20] calibrated two parameters, Mean Center Position distance difference (MCPD) and particles' Standard Deviational Ellipses (SDEs), to evaluate the performance of Lagrangian transport model with different coefficient combinations, and forecast the diffusion of the oil slick.

2. Study areas and remote sensing monitoring methods

Remote sensing data in coastal disasters monitoring and prevention has the characteristics of large area, real-time, using the method of remote sensing monitoring of red tides and sea-level rise, oil spilling has many effective results. This paper, using remote sensing data inversion and interpretation results as an example, introduces several methods of monitoring coastal disasters.

2.1. Study area

Hainan Province is located in the southernmost part of China, Hainan Island is the second largest island in China, and is separated from mainland by Qiongzhou Strait. It belongs to the tropical monsoon climate. Most of the coastal waters of Hainan Island are open sea areas with large waves, and the average wave height of 0.5–1.5 m. Hainan Island blows southeast wind and southwest wind in summer. There are more typhoons with the speed is extremely unstable. The average wind speed is 25 m/s. It can reach 30–60 m/s with the super typhoon. Hainan Province is the largest province in China suffering from marine disasters. The areas of disaster are mainly concentrated along the coastline of Hainan Island. The main disasters are storm surge, catastrophic waves, tsunami, red tide and coastal degradation caused by rising sea-level. Storm surge is due to strong atmospheric disturbances, such as the phenomenon of abnormal sea surface caused by strong winds or air pressure changes. If it superimposes with natural high tide, it will result in tidal surge, seawater immersion inland, even lead to catastrophe. The storm surges in Hainan Province usually occurs in summer and autumn, mainly caused by tropical cyclones, and more than the warning line of storm surge is 0.6 times. Catastrophic waves usually refer to the catastrophic waves that mean sea waves up to 6 meters above the waves. It can often overthrow the ship, destroy marine engineering and coastal engineering, and bring disasters to navigation, maritime construction, maritime military activities and fishing. Catastrophic waves are mainly caused by tropical cyclones and cold air in South China Sea, cold weather in winter is more likely to produce catastrophic waves. The Tsunami is usually caused by a seabed earthquake that is less than 100 kilometers beneath the seabed and more than 6.5 on the Richter scale. Underwater or coastal landslides or volcanic eruptions may also cause a Tsunami. There was a Tsunami caused by an earthquake in Hainan Island in January 1992. Tsunami wave speed as high as 700–800 km/h, and cross the ocean in a few hours. The wavelength can be up to hundreds of kilometers, and can travel thousands of miles with low loss energy. The ocean waves are less than a meter high, but when they reach the shallow coastal waters, the wavelengths decrease and the wave height increases dramatically. Tsunami forms a "water wall" with great energy up to tens of meters. Red tide is an anomalous phenomenon in marine ecosystems. Under certain environmental conditions, some phytoplankton, protozoa or bacteria in the seawater are proliferated or highly aggregated to cause the water to discolor a harmful ecological phenomenon. When the large amount of nutrients containing domestic sewage, industrial waste water and agricultural wastewater into the ocean, resulting in seawater eutrophication, red tide organisms will be rapidly multiply, they formed a red tide. Excessive amounts of phytoplankton consume the oxygen in seawater, and the dead phytoplankton release harmful substances that kill other creatures by hypoxia or

poisoning. The formation of red tide can be divided into four stages: start, development, maintenance and extinction. Water temperature and sewage content of inorganic matter are the main factors causing the red tide, but the topography is also an important factor. Sea-level rise is caused by global warming, polar glaciers melting, upper oceanic thermal expansion and other causes of global sea-level rise phenomenon. Sea-level rise leads to coastal degradation, mangrove disappearance, and coastal ecological damage. The Hainan Island study area remote sensing image is shown in **Figure 1**.

The geographical conditions of Bohai Sea and South China Sea are very different. The three sides of the Bohai sea are surrounded by land, and the whole shape of the Bohai coastline is similar to gourd. The Bohai Sea of gourd mouth is only 59 nautical miles, and the average depth of Bohai Sea is 25 m. Bohai Sea is more closed terrain, reducing the stormy storms, and the exchange rate with the ocean is slow, so it is a natural farm and natural harbor. However, a large number of ships parked and oil spill accident cause the Bohai oil pollution more and more serious. Human activities lead to about 10 million tons of oil into the ocean per year according to incomplete statistics, and the data accounts for about 0.5% of the world's annual oil production. There are 1 million to 1.5 million tons of oil is due to shipping operations and ship accidents into the ocean among them. Oil pollution is mainly caused by the oil industry, shipbreaking wastewater discharge, oil transport vessel cleaning, accidents and oil production
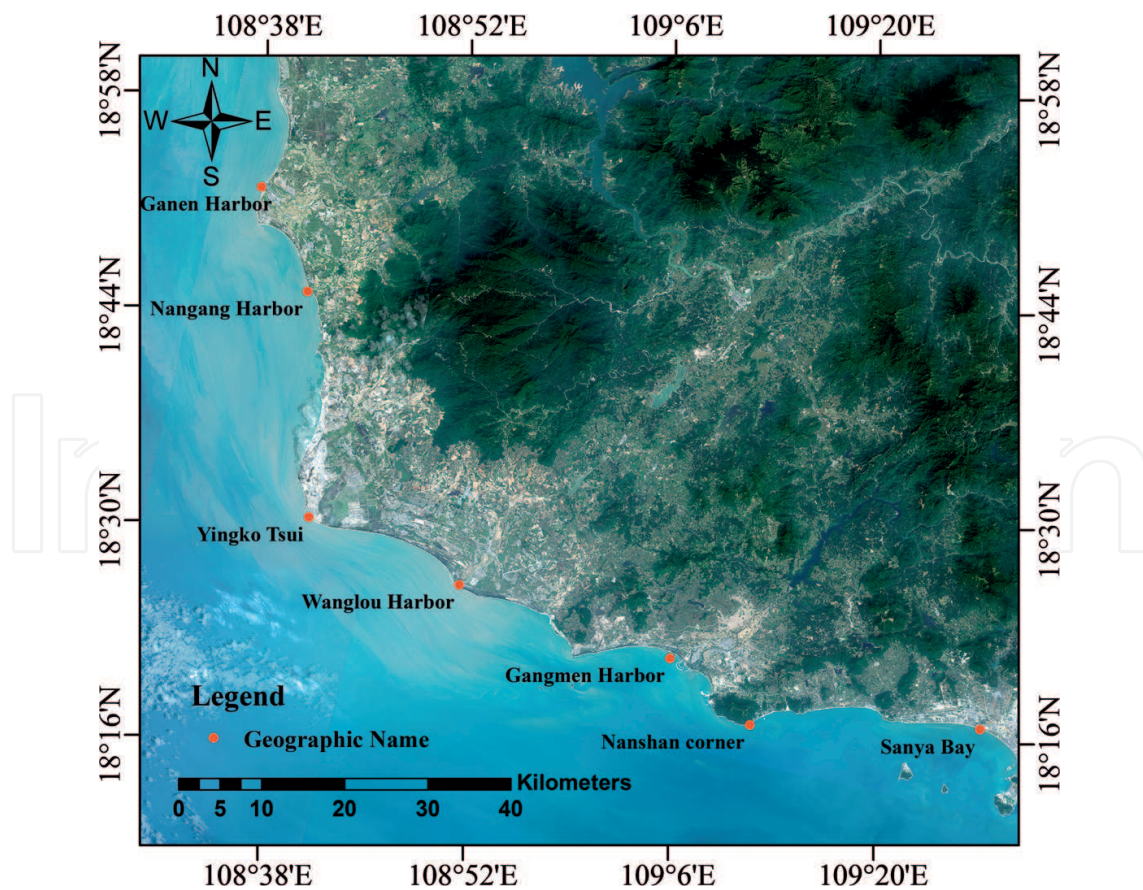

Figure 1. Hainan Island study area map.

at sea. It not only destroyed the coastal scenery, but also seriously endanger marine life. Bohai bathymetry map and the locations of PL19-3 B and C platforms are shown in **Figure 2**.

2.2. Data

In this paper, five kinds of optical data and one kind of microwave data are used. The optical data are MODIS, Spot6, Landsat 7 ETM, Landsat6 ETM, Landsat1 MSS and the microwave data is ASAR. The date, spatial resolution, wavelength range of remote sensing data used in this paper are in **Table 1**.

2.3. Red tide monitoring

Nutrient concentration and temperature are two major factors of the outburst of red tides, but upwelling also can bring nutrient with lower temperature, so the chlorophyll-a concentration inversion using remote sensing data is more suitable for coastal zone to forecast red tide. Coastal water chlorophyll-a concentration inversion is based on the Case 2 chlorophyll-a algorithm, which include empirical model and semi-analytical, bio-optical model of the water-leaving radiance Rrs(λ) [8, 21–23]. The empirical model utilizes the linear regression method to build model describing the relationship between chlorophyll-a concentration and Rrs(λ). Relatively, the semi-analytical, bio-optical model have two free variables, the absorption coefficient due to phytoplankton at 675 nm, aψ (675),and the absorption coefficient due to colored dissolved organic matter (CDOM) at 400 nm, ag(400). Although the semi-analytical,
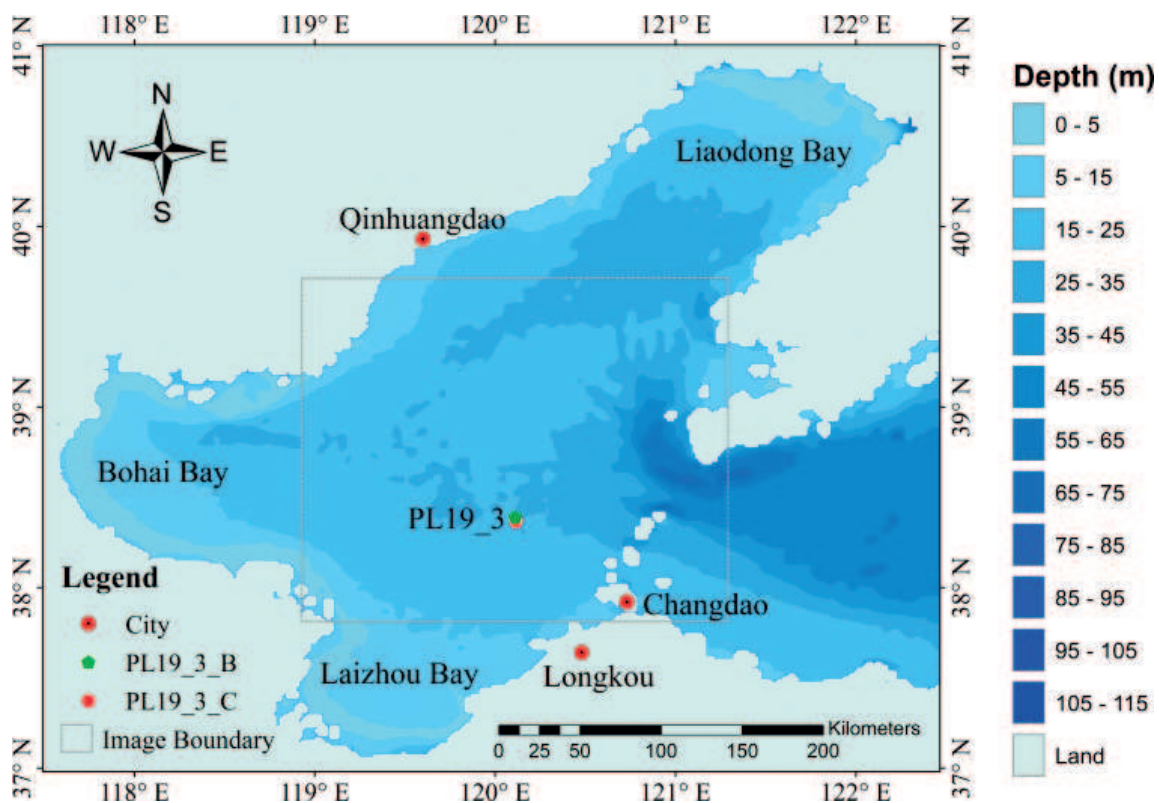

Figure 2. Bohai Bay study area map.

Data	Date	Spatial resolution (m)	Wavelength range (μm)
MODIS	2/3/2015	250	0.62–0.92
SPOT6	22/1/2013	1.5	0.45–0.75
Landsat6 ETM	24/2/2001	30	0.57–1.75
Landsat1 MSS	15/1/1973	80	0.5–11
ASAR	5/11/2011	150	5.6×10^4
	13/5/2001		
	14/5/2001		
	19/5/2001		

Table 1. Used remote sensing data.

bio-optical model with the inherent optical properties, it does not work well in the coastal zone effected heavily by suspended sediment. We choose an improved OC3M model using more high spatial resolution MODIS data (band 1, 2).

2.3.1. OC₃M model

A blue green ratio experience algorithm of CZCS developed by NASA such as Eq. (1), was the earliest model to calibrate pigment (including chlorophyll-a and brown pigment) concentration. A and B in Eq. (1) are empirical parameters, and C is pigment concentration.

$$C = A \left[\frac{R(433)}{R(550)} \right]^B \tag{1}$$

The MODIS chlorophyll-a production provides multiband algorithm, OC3M model, which is the most widely used empirical algorithm for MODIS data, such as Eqs. (2) and (3).

$$\log [Chla] = a_0 + a_1{}^*X + a_2{}^*X^{\wedge 2} + a_3{}^*X^{\wedge 3} + a_4{}^*X^{\wedge 4} \tag{2}$$

$$X = \log \left[\frac{\max(R_9, R_{10})}{R_{12}} \right] \tag{3}$$

where a_0, a_1, a_2, a_3 are undetermined coefficients, R_9, R_{10}, R_{12} are the reflections of MODIS band 9, band 10, band 12.

2.3.2. Provided OC₃M model

In order to obtain more accurate resolution inversion results, and as a result of lack of MODIS nearshore chlorophyll product, we decided to adopt OC3M model improved by 1/2 band, which is more suitable for nearshore areas. Then, we use two kinds of data to establish model, the one is MODIS water-color product, the other one is South China Sea measured value, and finally, we contrast and analysis the model accuracy.

2.3.2.1. Inverting model MODIS water color production

First of all, the two-band reflectivity model is established by the reflectance of the red-band and near-infrared bands of MODIS data (n = 1, 2), X_1 is ratio of two-band (Eq. (4)), X_2 is vegetation index (Eq. (5)).

$$X_1 = R_2/R_1 \tag{4}$$

$$X_2 = (R_2 - R_1)/(R_2 + R_1) \tag{5}$$

Chlorophyll concentration (Eq. (6)) is calculate by linear regression analysis using (n = 1, 2) and MODIS chlorophyll product provided by NASA Ocean Color Processing Center (http://oceancolor.gsfc.nasa.gov/cms).

$$Chla = b_1 \times X_n^{\wedge 3} + b_2 \times X_n^{\wedge 2} + b_3 \times X_n + b_4 \tag{6}$$

Stepwise regression analysis is used to input each band's information into the model and to carry out the significant tests of the band taken into the model. The model will test the significance of the front band, simultaneously, delete the bands whose significance is decreasing due to later band adding. The eventual band is the optimal one. Due to the stepwise regression analysis can evaluate the significance of bands, the model is selected in this paper. The inverting model, such as Eq. (7), acquired by the stepwise regression analysis of the spectral data (red spectral band, near-infrared band) and MODIS chlorophyll-a production.

$$Chla = c_1 \times R_1 + c_2 \times R_2 + c_3 \tag{7}$$

In Eq. (7), *Chla* is chlorophyll-a concentration, b_1, b_2, b_3, b_4, c_1, c_2, c_3 are undetermined parameters, R_1, R_2 are the reflection data of MODIS red band and near-infrared band.

2.3.2.2. Inverting model of measured southern China Sea data

The inverting model of measured Southern China Sea also need calculate the X_n (n = 1, 2)in Eqs. (4) and (5). The different part is the chlorophyll-a concentration data modeling that comes from measured Southern China Sea data.

$$Chla = d_1 {}^* X_n^{\wedge 3} + d_2 {}^* X_n^{\wedge 2} + d_3 {}^* X_n + d_4 \tag{8}$$

$$Chla = e_1 {}^* R_1 + e_2 {}^* R_2 + e_3 \tag{9}$$

In Eqs. (8) and (9), *Chla* is chlorophyll-a concentration (μg/L), d_1, d_2, d_3, d_4, e_1, e_2, e_3 are undetermined parameters during the regression analysis.

2.4. Sea-level rise

Sea-level rise caused by global climate change has significant impacts on coastal zone. Coastal ecosystems are particularly sensitive to sea-level rise, which is gradually causing the coastline to degenerate, and the area of mangroves to reduce or even disappear. Traditional remote

sensing methods to detect sea-level changes mostly use active microwave radar including altimeter, scatterometer and synthetic aperture radar to measure sea surface height, significant wave height, sea surface topography, simultaneously measure the ocean current, sea wave, tide, sea surface wind. Nonetheless, the spatial resolution of microwave data is much lower than the visible data, which is more suitable for the coastal zone research. Coastline changes without anthropogenic impact can be used to estimate sea-level changes. The interpretation of coastline based on the different interpretation marks of coastline types, and the main types of southwest of Hainan island include sandy coastline, rocky coastline, estuary coastline and artificial coastline. This part will introduce the interpretation marks of different coastline.

2.4.1. Sandy coastline

The mark of the sandy shoreline is the highest traced line consisting of small gravel, coarse sand, shell debris, driftwood, water grass at the foot of the lateral coastal sand bank. **Figure 3** is the sandy coastline in SPOT6 and outside picture.

2.4.2. Rocky coastline

The rocky coastlines are divided into the one with beach and without beach. Although both of the water edge of rocky coastlines have seabed, the trace line of coastline with beach is the same as the one of sandy coastline (**Figure 4**). The trace line of coastline without beach is below the latest sea cliff (**Figure 5**).

2.4.3. Estuary coastline

The estuary coastline has two parts: the boundary between sea and land; the boundary between sea and river. The interpretation mark of former is vegetation on the land edge, and the latter is the suddenly broadening line between sea and river, such as **Figure 6**.

2.4.4. Artificial coastline

The main artificial coastlines of the research area are mariculture and artificial pier. The interpretation mark is artificial building, such as **Figure 7**.
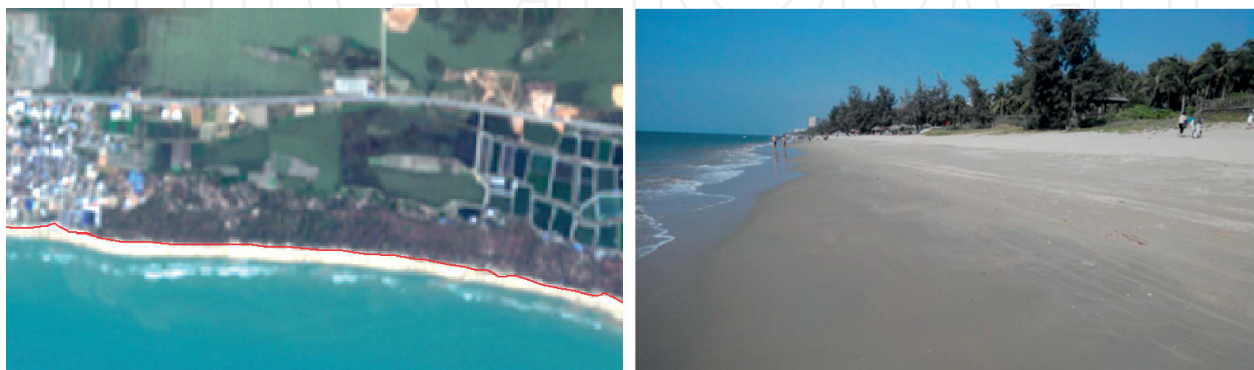

Figure 3. Sandy coastline in SPOT6 and outside picture.

Figure 4. Rocky coastline with beach in SPOT6 and outside picture.

Figure 5. Rocky coastline without beach in SPOT6.

Figure 6. Estuary coastline in SPOT6.

Figure 7. Artificial coastline in SPOT6.

2.5. Oil spilling trajectory simulation model

The oil spilling trajectory simulation can help predict the area where the oil spill might reach and where it might be contaminated. However, the Lagrange model is available (such as Eqs. (10)–(11)).

$$x_i^{(t+\Delta t)} = x_i^t + v_i \Delta t \tag{10}$$

$$v = C_c u_c + C_D D_W u_W + C_H u_H + u_d \tag{11}$$

where parameters x_i^t *and* $x_i^{t+\Delta t}$ are the locations of oil particles at t and $t + \Delta t$ moment, Δt is time interval setting Δt equal 1 h in the text. When the model forecasts the oil trajectory, the symbol of Δt is plus; when the model traces oil trajectory, the symbol of Δt is minus. Parameter v_i is the drifting speed of oil particle i at the t moment. The location of each oil particle calculated as the linear combination of wind velocity, current velocity, wave-induced Stokes drift and turbulent diffusive velocity. Where C_c is current drift coefficient, u_c is the surface current velocity, C_D is wind drag coefficient, D_W is the transformation matrix taking the wind deflection angle into account, u_w is wind velocity above sea surface 10 m, C_H is wave-induced Stokes drift coefficient, u_H is wave-induced Stokes drift velocity. C_c, C_D, C_H are empirical parameters reducing the model accuracy. However there are some methods using the buoy data and monitoring data on correcting the oil trajectory correction at present, the data cannot be obtained timely.

Aiming at this problem, we calibrate Lagrangian numerical model with remote sensing image to improve Lagrangian model, which is independent of weather, climate and low cost. We correct the Lagrangian model using to simulate the oil spilling based on the ENVISAT ASAR remote sensing data which time phase is during the PL19-3 oil spilling accident on Bohai. The oil simulation trajectory is made of points by remote sensing data inverting results. In **Figure 7**, the points D, E, I are the oil slick locations of remoting sensing image on June 11, June 13, June

14 respectively. The simulation points constitute the oil trajectory. The oil slick D acts as the testing trajectory to correct the simulation result.

Eventually, we use the ellipse center and the ellipse long axis of oil slick area to evaluate the simulation result. The center of ellipse calculation method is in Eqs. (12) and (13), the long axis of ellipse calculation method is in Eq. (14).

$$\overline{X} = \frac{1}{n}\sum_{i=1}^{n} x_i \tag{12}$$

$$\overline{Y} = \frac{1}{n}\sum_{i=1}^{n} y_i \tag{13}$$

$$\tan\theta = \frac{\left(\sum_{i=1}^{n} x_i^2 - \sum_{i=1}^{n} y_i^2\right) + \sqrt{\left(\sum_{i=1}^{n} x_i^2 + \sum_{i=1}^{n} y_i^2\right) + 4\left(\sum_{i=1}^{n} x_i y_i\right)^2}}{2\sum_{i=1}^{n} x_i y_i} \tag{14}$$

3. Result and discussion

3.1. Chlorophyll-a inverting result

Through the chlorophyll-a inverting result (**Figure 8**) in the southwest Hainan Island, we can see the distribution regularities. The high concentration of chlorophyll-a is found near the
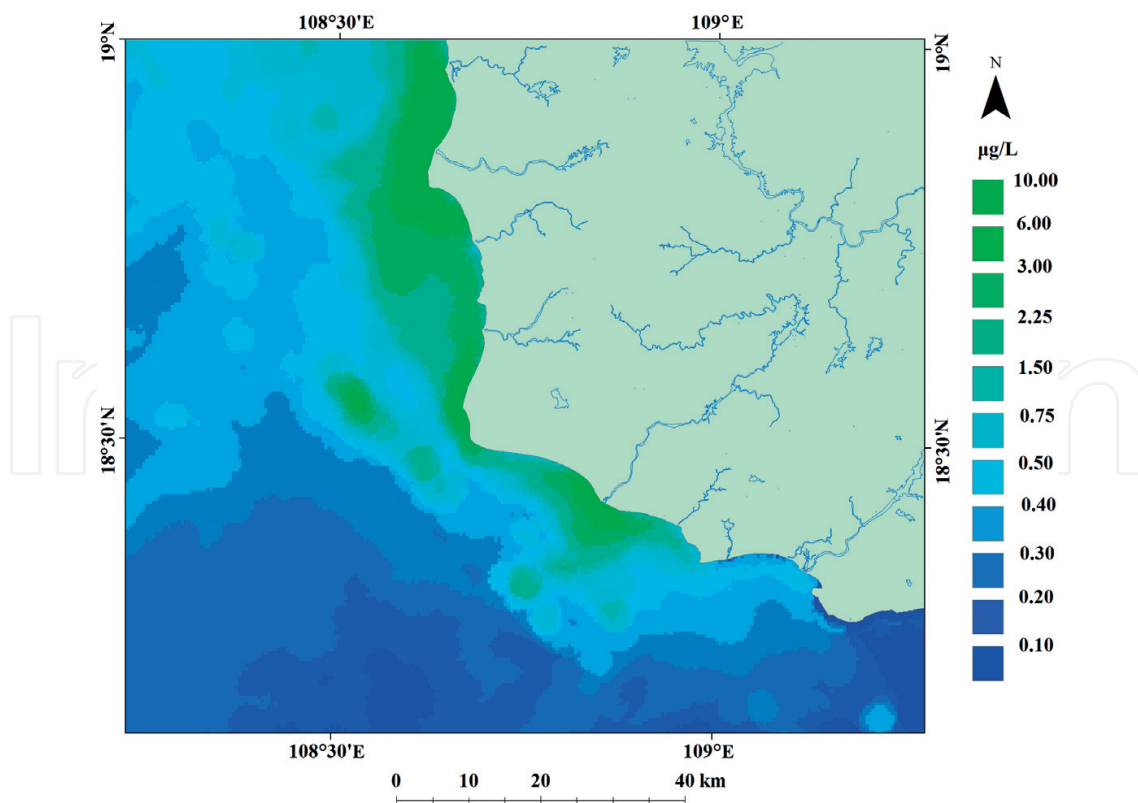

Figure 8. Chlorophyll a inverting result.

estuary. But the magnitude is not completely related to the distance of the estuary, so there are other reasons for that. We add the contours of the water depth and the chlorophyll-an inversion result to discuss the relationship between the shallow water terrain and chlorophyll-a concentration.

We add the counter of water depth and chlorophyll-a concentration. In order to see the relationship between the two parts, we enlarge three parts of **Figure 8** in **Figure 9**. The adding results suggest that, in normal condition, the chlorophyll-a concentrate is higher than 2.25 µg/L in the depth lower than 15 m, and lower than 0.75 µg/L in the depth higher than 20. In the c of **Figure 9**, the concentration is low (<0.75 µg/L) near the estuary. Maybe the slop of shallow water terrain is larger than other coastal zone.

3.2. Sea-level rise

The coastline interpretation results in **Figure 10** show that the coastline without anthropogenic influence whose main part is sandy coastline is deteriorating year by year. The most heavily
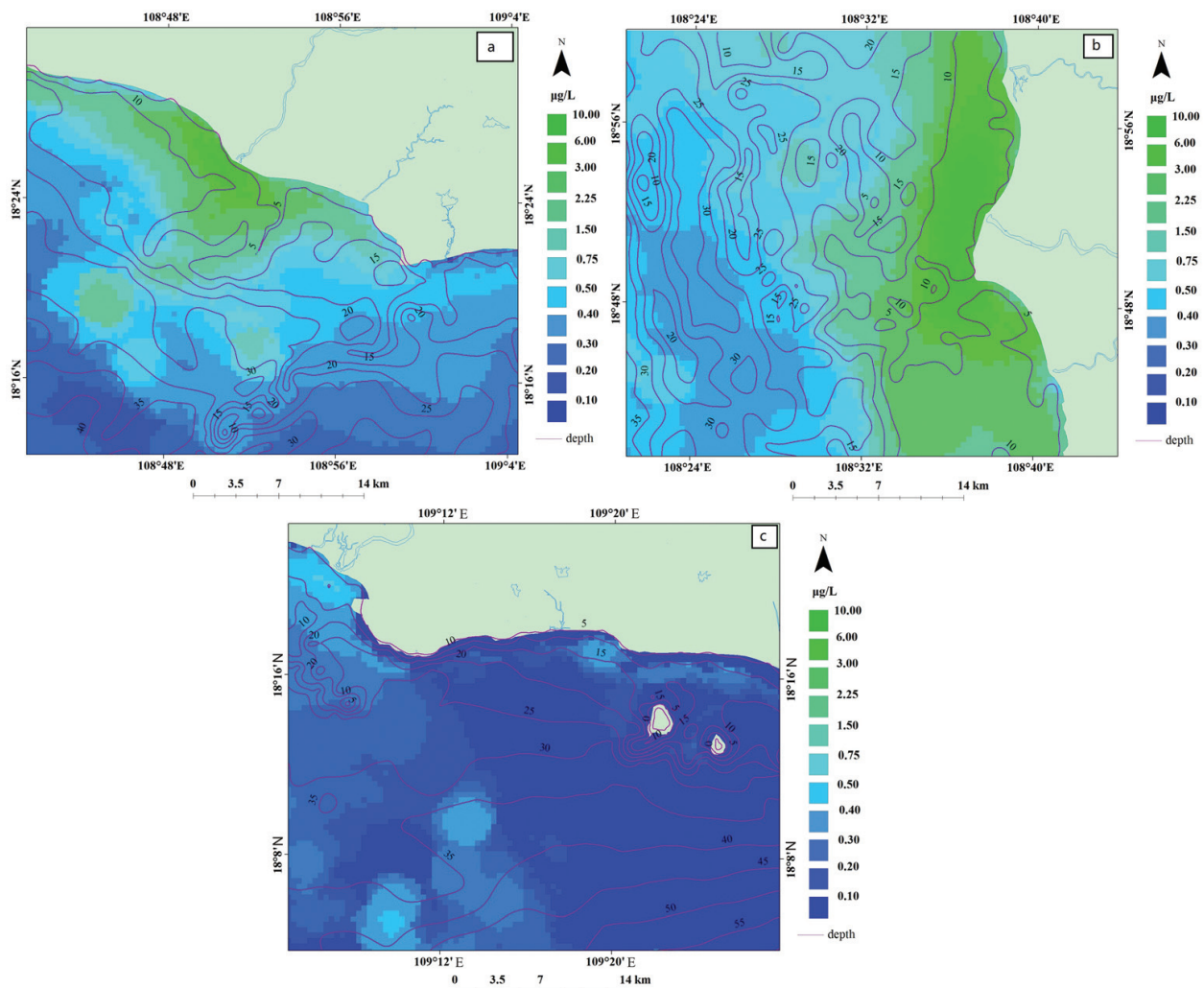

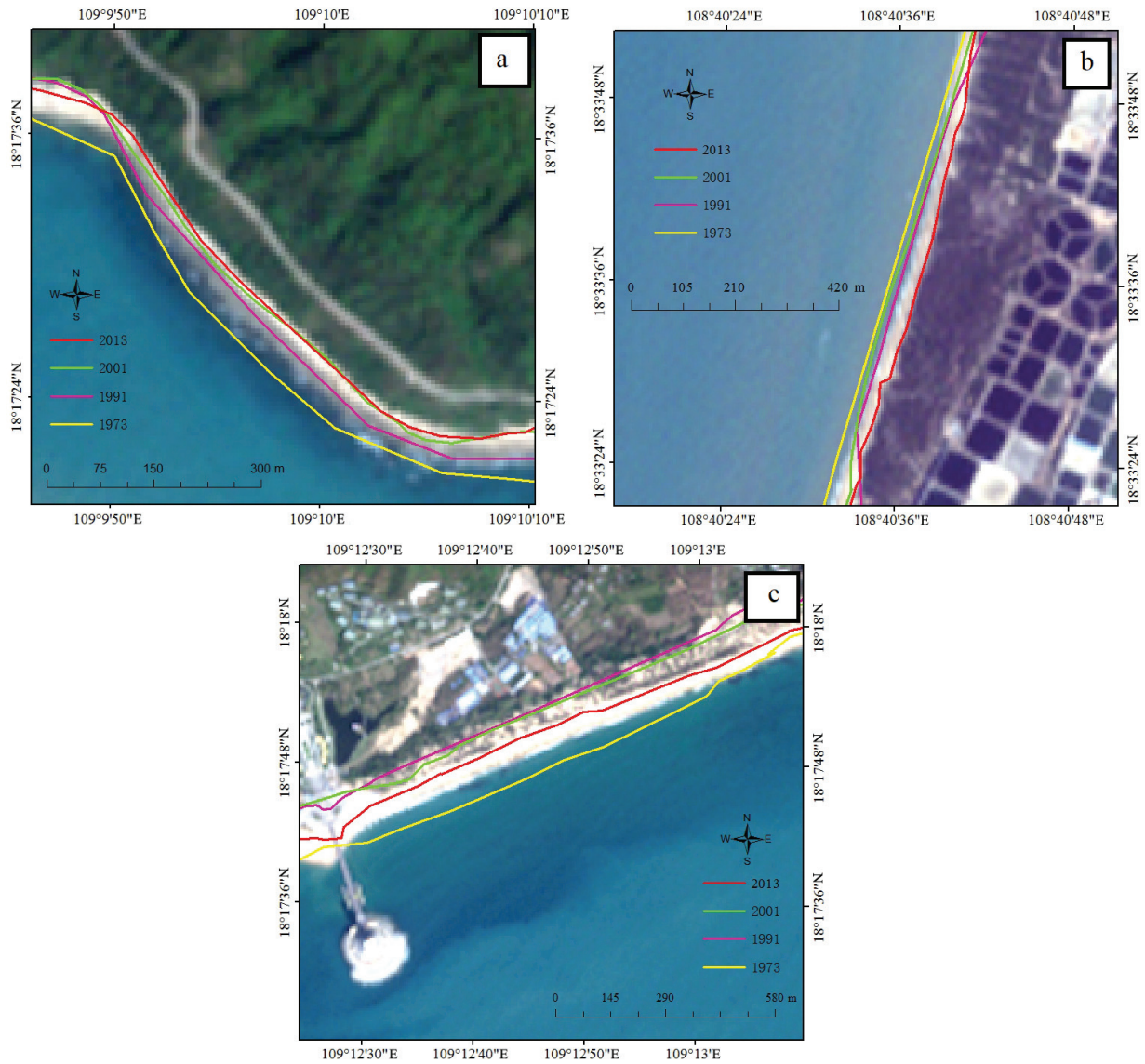**Figure 9.** Water depth and chlorophyll a concentration adding.

Figure 10. Sandy coastline changes between 1973 and 2013.

eroded part of up to more than 30 m from 1973 to 2013. Some part of the sandy coastline eroded from 1973 to 2013, but it was increasing from 1991 to 2013, such as the c of **Figure 10** because of the reclaiming land from the sea.

3.3. Oil spilling trajectory simulation

Figure 11 is comparison of the oil slick simulation trajectory (points) and oil actual location (irregular polygon). The result shows that oil slick simulation and real oil slick are similar in distributional pattern and location. In the third figure of **Figure 11**, the location of oil slick is accordance with real oil slick moving with current, but the model can simulate the oil slick staying in the area where the accident occurred.
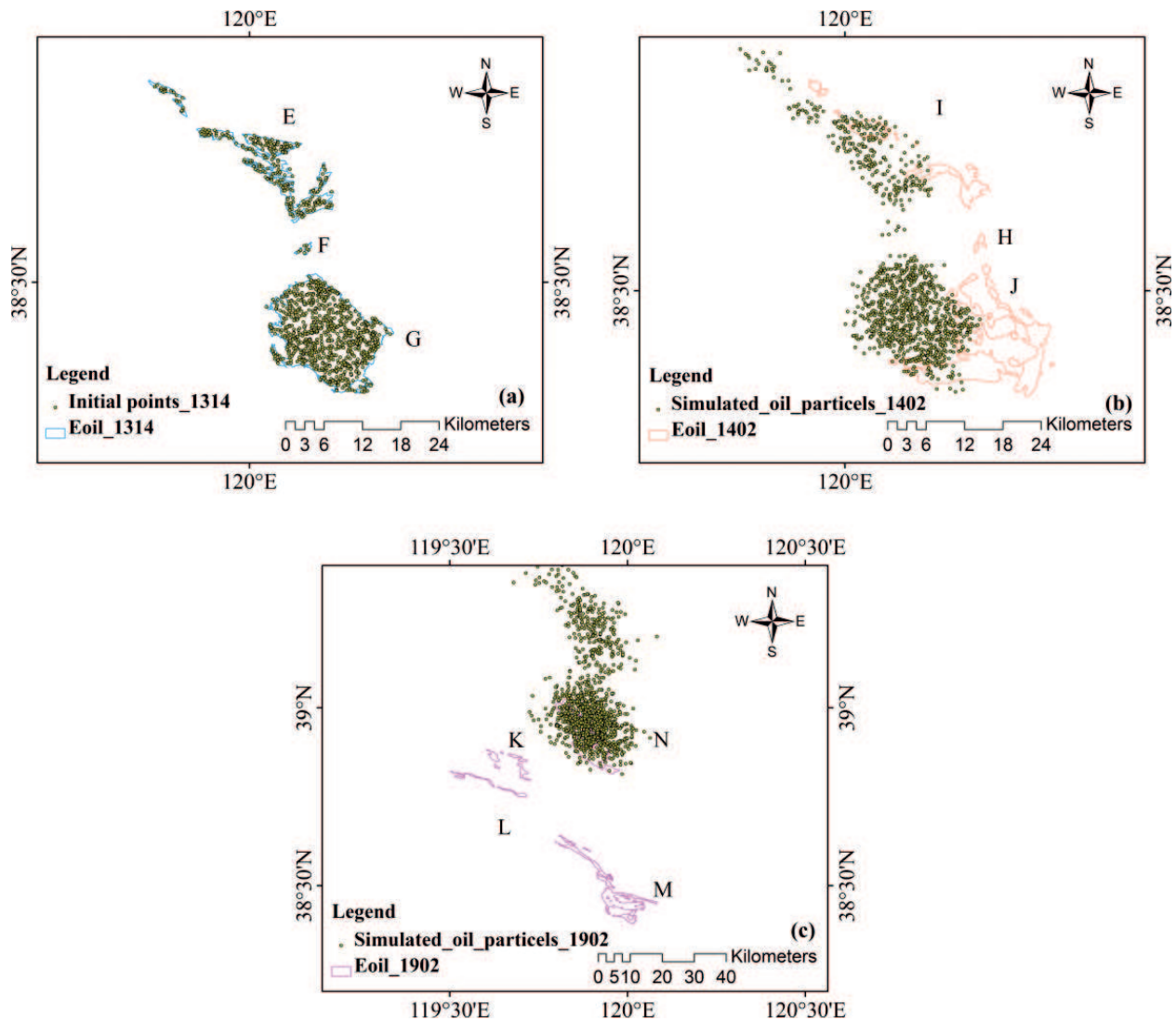
Figure 11. The distribution of simulation particles with calibrated model with start particle on June 13 (Note: Initial points_1314 means that the initial points are distributed at UTC 14:00 on June 13 and simulated_oil_particles_1402 means t that these simulated oil particles are obtained as the moment of UTC 02:00 on June 14).

3.4. Coastal infrastructure

Along with the rapid development of coastal cities, the number of human activities is increasing, so the planning and construction of the coastal infrastructures become increasingly important in the terms of coastal ecological protection, aquaculture, marine transport and so on. The constructions of different coastal infrastructures are based on the different types of coasts, which include bedrock coast, plain coast and biological coast. Bedrock coast include cape and bay, and many bedrock coasts are natural deep harbor. There are three kinds of plain coasts: muddy coast, sandy coast and deltaic coast. Most of the plain coasts are straight, and the terrains are flat, and thus are suitable for building saltern, lidos and the fisheries. Biological coast is divided into two kinds of mangroves and coral reefs. As the biological coasts have the function of protecting biological diversity and wetlands, this kind coasts should not be set up large coastal infrastructures. Although nearshore ecological environment is of great
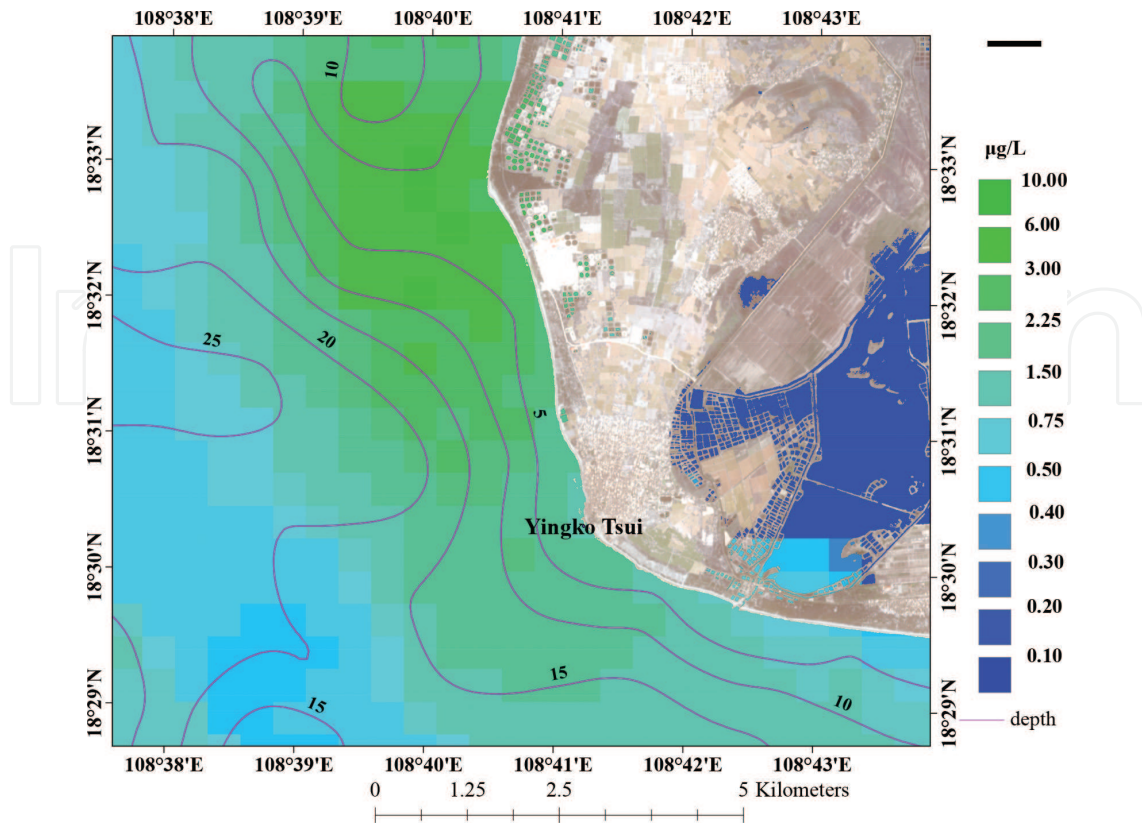
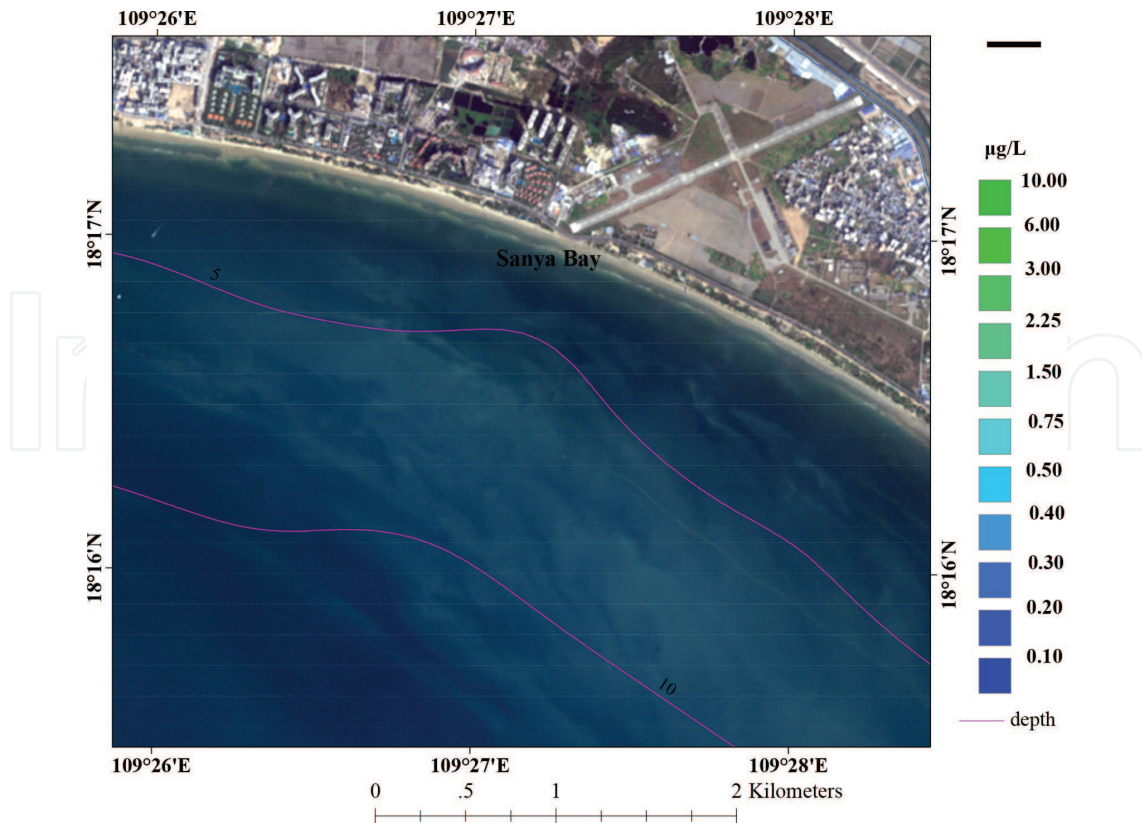**Figure 12.** The biggest saltern in China Yingge saltern image.

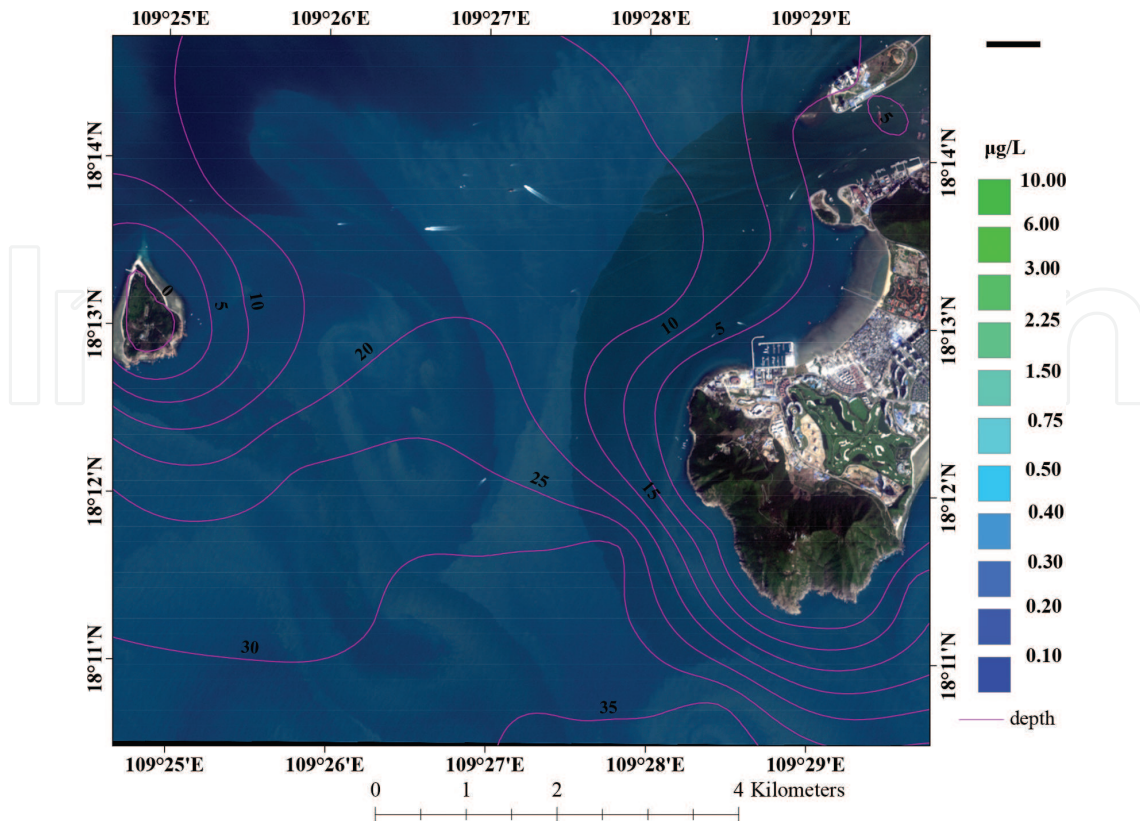
Figure 13. Sanya Bay lido image.

Figure 14. Suitable location for deep harbor image.

significance to human beings, the pollution of coastal water by inland waters and the changing of the coastline through reclamation works destroy the coastal biodiversity.

The coastal infrastructure planning also should consider the coastal disaster factors. The high chlorophyll-a concentration coastal zone usually with a gentle bottom topography need to reduce the discharge of sewage. These coastal regions can be used to build saltern, such as **Figure 12**. The shallow water regions with steep bottom topography have lower chlorophyll-a concentration and clear water. These regions with sandy coastline are suitable for lido, such as **Figure 13**; the ones with rocky coastline are suitable for deep harbor, such as **Figure 14**. The remote sensing methods forecast the area where disaster may occur, and make coastal infrastructure construction more reasonable.

4. Conclusion

Overall, we have inversed chlorophyll-a centration and coastline interpretation in southwest Hainan Island, and used the improved Lagrangian model to simulate the oil slick movement trend and distribution. Through the research in this paper, we acquire a couple of conclusions.

1. The adding of chlorophyll-a centration and counter of shallow water depth suggest that not only the nutrient salt brought by the land runoff and temperature are the main reasons for the increase of chlorophyll concentration, but also the shallow Marine terrain in the nearshore area is an important factor.

2. The coastline is degenerating in 40s from 1973 to 2013, and the most heavily eroded part of up to more than 30 m. The sea-level is rising year by year.

3. The oil slick trajectory result suggest that a part of oil slick moves with the current, and the other part stays in the area where the accident occurred. The improved Lagrangian model can simulate the trajectory of oil slick efficiently, but it is not suitable for prediction of the part of oil slick which does not move with current.

4. The remote sensing methods can forecast the area where coastal disasters caused by human activity may occur, and interpret the types of coastline. The remote sensing data application can help to make coastal infrastructure construction planning more reasonable.

Author details

Yan Yu[1]*, Shengbo Chen[1], Tianqi Lu[1] and Siyu Tian[2]

*Address all correspondence to: yuyan14@mails.jlu.edu.cn

1 College of Geo-exploration Science and Technology, Jilin University, Changchun, China

2 Institute of Remote Sensing and Digital Earth, Chinese Academy of Sciences, Beijing, China

References

[1] Doucette GJ, Turner JT, Powell CL, et al. Trophic accumulation of PSP toxins in zooplankton during *Alexandrium fundyense*, blooms in Casco Bay, Gulf of Maine, April–June 1998. I. Toxin levels in *A. fundyense*, and zooplankton size fractions. Deep Sea Research Part II: Topical Studies in Oceanography. 2005;**52**(19-21):2764-2783. DOI: 10.1016/j.dsr2.2005.06.031

[2] Moisan JR, Moisan TA, Abbott MR. Modelling the effect of temperature on the maximum growth rates of phytoplankton populations. Ecological Modelling. 2002;**153**(3):197-215. DOI: 10.1002/ecy.1581

[3] Huang WG, Lou XL. AVHRR detection of red tides with neural networks. International Journal of Remote Sensing. 2003;**24**(10):1991-1996. DOI:10.1080/0143116031000068213

[4] Steidinger KA, Haddad K. Biologic and hydrographic aspects of red tides. Bioscience. 1981;**31**(11):814-819. DOI: 10.2307/1308678

[5] Pinkerton MH, Richardson KM, Boyd PW, et al. Intercomparison of ocean colour band-ratio algorithms for chlorophyll concentration in the subtropical front east of New Zealand. Remote Sensing of Environment. 2005;**97**(3):382-402. DOI: 10.1016/j.rse.2005.05.004

[6] Mao XM, Huang WG. Algorithms of multiband remote sensing for coastal red tie waters. Chinese Journal of Applied Ecology. 2003;**14**(7):1200-1202

[7] Morel A, Ahn YH. Optical efficiency factors of free-living marine bacteria: Influence of bacterioplankton upon the optical properties and particulate organic carbon in oceanic waters. Journal of Marine Research. 1990;**48**(1):145-175. DOI: 10.1357/002224090784984632

[8] Morel A, Ahn YH. Optics of heterotrophic nanoflagellates and ciliates: A tentative assessment of their scattering role in oceanic waters compared to those of bacterial and algal cells. Journal of Marine Research. 1991;**49**(1):177-202. DOI: 10.1357/002224091784968639

[9] Morel A, Bricaud A. Theoretical results concerning light absorption in a discrete medium, and application to specific absorption of phytoplankton. Deep Sea Research Part A Oceanographic Research Papers. 1981;**28**(11):1375-1393

[10] Li SS, Meng XW, Ge ZM, et al. Vulnerability assessment on the mangrove ecosystems in qinzhou bay under sea level rise. Acta Ecologica Sinica. 2014;**34**(10):2702-2711. DOI: 10.5846/stxb201309032200

[11] Yao TD, Liu SY, et al. Recent glacier retreat in Central Asia and its impact on water resources in Northwestern China. Science in China (Series D). 2004;**4**(6):535-543. DOI: 10.1360/03yd0256

[12] Surazakov AB, Aizen VB. Estimating volume change of mountain glaciers using SRTM and map-based topographic data. IEEE Transactions on Geoscience & Remote Sensing. 2006;**44**(10):2991-2995. DOI: 10.1109/TGRS.2006.875357

[13] Thomas HS, Dahe Q, Gian-kasper P, et al. Climate Change 2013: The Physical Science Basis: Working Group I Contribution to the Fifth Assessment Report of the Intergovernmental Panel on Climate Change. IPCC ed. Cambridge: Cambridge University Press; 2014. 203 pp

[14] Radić V, Hock R. Regionally differentiated contribution of mountain glaciers and ice caps to future sea-level rise. Nature Geoscience. 2011;**4**(2):91-94. DOI: 10.1038/NGEO1052

[15] Jacob T, Wahr J, Pfeffer WT, et al. Recent contributions of glaciers and ice caps to sea level rise. Nature. 2012;**482**(7386):514-518. DOI: 10.1038/nature10847

[16] Bouchahma M, Yan W. Automatic measurement of shoreline change on Djerba Island of Tunisia. Computer & Information Science. 2002;**5**(5):17-24. DOI: 10.5539/cis.v5n5p17

[17] Xu HQ. A study on information extraction of water body with the modified normalized difference water index (MNDWI). Journal of Remote Sensing. 2005;**9**(5):589-595

[18] Galt JA. Trajectory analysis for oil spills. Journal of Advanced Marine Technology Conference. 1994;**11**:91-126

[19] Reed M, Øistein J, Brandvik PJ, et al. Oil spill modeling towards the close of the 20th century: Overview of the state of the art. Spill Science & Technology Bulletin. 1999;**5**(98): 3-16. DOI: 10.1016/S1353-2561(98)00029-2

[20] Tian SY, Huang XX, Li HG. A new method to calibrate Lagrangian model with ASAR images for oil slick trajectory. Marine Pollution Bulletin. 2016;**116**(1):95-102. DOI: 10.1016/j.marpolbul.2016.12.054

[21] Lee Z, Carder KL, Hawes SK, et al. Model for the interpretation of hyperspectral remote-sensing reflectance. Applied Optics. 1994;**33**(24):5721. DOI: 10.1364/AO.33.005721

[22] Morel A, Gentili B. Diffuse reflectance of oceanic waters. II. Bidirectional aspects. Applied Optics. 1993;**32**(33):6864-6879. DOI: 10.1364/AO.32.006864

[23] Lee Z, Carder KL, Hawes SK, et al. Model for the interpretation of hyperspectral remote-sensing reflectance. Applied Optics. 1994;**33**(24):5721-5732. DOI: 10.1364/AO.33.005721